sustainability

MDPI

Article

Applying Artificial Neural Network and Response Surface Method to Forecast the Rheological Behavior of Hybrid Nano-Antifreeze Containing Graphene Oxide and Copper Oxide Nanomaterials

Ammar A. Melaibari [1,2], Yacine Khetib [1,3], Abdullah K. Alanazi [4], S. Mohammad Sajadi [5,6], Mohsen Sharifpur [7,8,*] and Goshtasp Cheraghian [9,*]

1 Mechanical Engineering Department, Faculty of Engineering, King Abdulaziz University, Jeddah 80204, Saudi Arabia; aamelaibari@kau.edu.sa (A.A.M.); ykhetib@yahoo.com (Y.K.)
2 Center of Nanotechnology, King Abdulaziz University, Jeddah 80204, Saudi Arabia
3 Center Excellence of Renewable Energy and Power, King Abdulaziz University, Jeddah 80204, Saudi Arabia
4 Department of Chemistry, College of Science, Taif University, P.O. Box 11099, Taif 21944, Saudi Arabia; aalshahri@tu.edu.sa
5 Department of Nutrition, Cihan University-Erbil, Kurdistan Region, Erbil 44001, Iraq; smohammad.sajadi@gmail.com
6 Department of Phytochemistry, SRC, Soran University, KRG, Soran 44008, Iraq
7 Department of Mechanical and Aeronautical Engineering, University of Pretoria, Pretoria 0002, South Africa
8 Department of Medical Research, China Medical University Hospital, China Medical University, Taichung 404, Taiwan
9 Independent Researcher, 38106 Braunschweig, Germany
* Correspondence: mohsen.sharifpur@up.ac.za (M.S.); goshtasbc@gmail.com (G.C.)

Abstract: In this study, the efficacy of loading graphene oxide and copper oxide nanoparticles into ethylene glycol-water on viscosity was assessed by applying two numerical techniques. The first technique employed the response surface methodology based on the design of experiments, while in the second technique, artificial intelligence algorithms were implemented to estimate the GO-CuO/water-EG hybrid nanofluid viscosity. The nanofluid sample's behavior at 0.1, 0.2, and 0.4 vol.% is in agreement with the Newtonian behavior of the base fluid, but loading more nanoparticles conforms with the behavior of the fluid with non-Newtonian classification. Considering the possibility of non-Newtonian behavior of nanofluid temperature, shear rate and volume fraction were effective on the target variable and were defined in the implementation of both techniques. Considering two constraints (i.e., the maximum R-square value and the minimum mean square error), the best neural network and suitable polynomial were selected. Finally, a comparison was made between the two techniques to evaluate their potential in viscosity estimation. Statistical considerations proved that the R-squared for ANN and RSM techniques could reach 0.995 and 0.944, respectively, which is an indication of the superiority of the ANN technique to the RSM one.

Keywords: hybrid nanofluid; viscosity; arterial neural network; response surface method

Citation: Melaibari, A.A.; Khetib, Y.; Alanazi, A.K.; Sajadi, S.M.; Sharifpur, M.; Cheraghian, G. Applying Artificial Neural Network and Response Surface Method to Forecast the Rheological Behavior of Hybrid Nano-Antifreeze Containing Graphene Oxide and Copper Oxide Nanomaterials. *Sustainability* **2021**, *13*, 11505. https://doi.org/10.3390/su132011505

Academic Editor: Anastasia V. Penkova

Received: 25 August 2021
Accepted: 11 October 2021
Published: 18 October 2021

1. Introduction

Heat transfer, given its various applications, has long been the focus of researchers and engineers [1,2]. Heat transfer can be attributed to the movement of free molecules, lattice vibration, molecular diffusion, as well as molecular collisions. Thermal conductivity is the potential of matter in heat transfer, so that materials with high thermal conductivity have a greater heat transfer rate [3,4]. Many studies have shown that the presence of nanoscale solids with high thermal conductivity can amplify the fluid thermal conductivity [5,6] and, consequently, intensify the heat transfer rate [7–13]. Considering the fluid motion in the convection heat transfer, in addition to the thermal conductivity, the viscosity can

also be effective in determining the convective heat transfer coefficient [14,15]. In the convection heat transfer scope, the fluid velocity field is required. To know the fluid velocity field, momentum conservation (Navier–Stokes equation) must be solved [16]. In the Navier–Stokes equation, there is friction force, which is itself a function of viscosity and velocity gradient. Therefore, knowledge of the viscosity changes is essential for solving convection heat transfer problems. Adding nanoparticles can have two significant effects on the viscosity; that is, an increase in viscosity and a change from Newtonian behavior to non-Newtonian behaviour [17,18]. From one perspective, studies on graphene-containing nanofluid are divided into viscosity, thermal conductivity, and other properties [19]. The number of studies on thermal conductivity is greater than studies on viscosity [20]. Table 1 summarizes the studies using graphene nanoparticles.

Table 1. Summary of studies using graphene.

References	Nanoparticles	Concentration\Temperature	Findings
Hu et al. [21]	$GN/EG-DW$ 60 : 40 vol.%		Investigation of pool boiling heat transfer (PBT) Up to 0.02 wt.%, PBT enhanced
Yu et al. [22]	GON/EG	0–5 vol.% 10–60 °C	$\frac{k_{nf}}{k_{bf}} = 1.61$
Yu et al. [23]	$GON-DW$ $GON-propyl\ glycol$ $GON-liquid\ paraffin$	0–5 vol.%	Owing to incorporation GON nanosheets into DW, propyl glycol, and liquid paraffin, k intensified by 30.2, 62.3, and 76.8%
Yu et al. [24]	GON/EG	5.0 vol.%	Enhancement in $\frac{k_{nf}}{k_{bf}}$ is up to 61.0%. It was found that the maximum enhancement was independent of temperature
Yu et al. [25]	GN/EG	5 vol.%	$\frac{k_{nf}}{k_{bf}} = 1.86$
Moghaddam et al. [26]	$Graphene–glycerol$	0.25–2 wt.% 20–60 °C	μ_{nf} ntensified up to 401.49% at 2 wt.% and 20 °C.
Ahammed et al. [27]	$Graphene–w$	0.05, 0.1, and 0.15 vol.% 10–50 °C	37.2% enhancement in thermal conductivity at 0.15 vol.%
Baby et al. [28]	$Graphene/EG-DI$	0.005–0.05 vol.% 25–50 °C	$\frac{k_{nf}}{k_{bf}} = 1.75$
Aravind and Ramaprabhua [29]	GN/EG $GN/DI\ water$	0.14 vol.% 25 °C	$\frac{k_{nf}}{k_{EG}} = 1.065$ $\frac{k_{nf}}{k_{DI\ water}} = 1.136$
Kole and day [30]	$GNP/EG-W$	0.041–0.395 $vol.\%$ 10–70 °C	viscosity increased by 100%

Given the relatively high thermal conductivity $\left(76.5\ \frac{W}{m.K}\right)$ of copper oxide (CuO), this nanoparticle has also been used in many studies. Table 2 summarizes the studies using copper oxide nanoparticles.

Hybrid nanofluids benefit from the advantages of two different nanoparticles, so many researchers have focused on this class of nanofluids [39–44]. The correlations used to estimate thermal conductivity or viscosity (for base fluids) are not accurate for nanofluids [45–48]. Conducting many experimental measurements on thermal conductivity or viscosity is costly as well as time-consuming [49,50]. Therefore, using predictive techniques can be helpful. In this way, algorithms based on artificial intelligence (ANN) and response surface methodology (RSM) have been widely used by researchers [51–53]. In Table 3, several studies including ANN/RSM approaches are summarized.

Table 2. Summary of studies using CuO.

References	Nanoparticles	Concentration\Temperature	References
Águila et al. [31]	CuO/Octadecane	30–55 °C 2.5, 5, and 10 wt.%	$\frac{\mu_{CuO/Octadecane}}{\mu_{Octadecae}} = 1.6$ non-Newtonian
Sahoo and Kumar [32]	Al_2O_3-CuO-TiO_2/water	0.01–0.1% 35 °C to 50 °C	$\frac{\mu_{Al2O3-CuO-TiO2/w}}{\mu_{Al2O3-CuO/w}} = 1.1725$ $\frac{\mu_{Al2O3-CuO-TiO2/w}}{\mu_{Al2O3-TiO2/w}} = 1.5541$
Esfe et al. [33]	CuO-MWCNT/10W40	5–55 °C Up to 10 vol.%	$\frac{\mu_{MWCNT-CuO/10W40}}{\mu_{10W40}} = 1.22$ Non-Newtonian
Akilu et al. [34]	TiO_2-CuO-C/EG	Up to 2 vol.% 30–60 °C	$\frac{\mu_{TiO2-CuO-C/EG}}{\mu_{EG}} = 1.80$ Newtonian
Asadi et al. [35]	CuO-TiO_2/water	0.1 to 1 vol% 25–55 °C	Newtonian behavior
Shah et al. [36]	CuO/EG-water (70;30)	0.3 vol.%	Newtonian
Priya et al. [37]	CuO–water	Up to 0.016 vol.% 28–55 °C	$\frac{\mu_{CuO/water}}{\mu_{water}} \sim 1.10$
Alawi et al. [38]	CuO/R134a	1 to 5 vol.%27–47 °C	$\frac{\mu_{CuO/R134}}{\mu_{R134}} \sim 3.47$

Table 3. Summary of studies including ANN/RSM approaches.

Reference	Nanofluid	Input Data/Output Variable	Temperature/Concentration	Accuracy	Methods
Zhao et al. [54]	Al_2O_3–water CuO–water	T, φ, ρ_{np} d_{np} *and* μ_{bf} output: μ_{nf}	10–50 °C up to 12 vol.%	$(R^2)_{Al2O3/water} = 0.9966$ $(R^2)_{CuO/water} = 0.9998$	ANN
Shahsavar and Bahiraei [55]	Fe_3O_4-CNTs/water	$T, \varphi_{Fe_3O_4}$ $\dot{\gamma}$ *and* φ_{CNTs} output: μ_{nf}	25 and 55 °C $0.1 < \varphi_{Fe_3O_4} < 0.9$ $0 < \varphi_{CNTs} < 1.35$	$R^2 = 0.999$	ANN
Ghaffarkhah et al. [56]	MWCNT-Al_2O_3/SAE40 MWCNT-MgO/SAE40 MWCNT-ZnO/SAE40 MWCNT-SiO_2/SAE40	T , φ μ_{nf}	25 and 50 ° 0.05, 0.25, 0.50, 0.75, and 1 vol.%	Not reported	ANN
Alirezaie et al. [57]	MWCNT-MgO/Engine oil	$T, \varphi, \dot{\gamma}/\mu_{nf}$	0.0625, 0.125, 0.25, 0.5, 0.75, and 1 vol.% 25–50 °C	$R^2 = 0.9973$	ANN
Yan et al. [58]	Graphene nanosheets/ethylene glycol	T, φ σ_{nf}	25–70 °C 0–5 wt.%	$R^2 = 0.981$	RSM
Tian et al. [59]	Al_2O_3-MWCNT/10W40	T, φ k_{nf}	25–65 °C Up to 1 vol.%	$R^2 = 0.9948$	RSM
Yan et al. [40]	MWCNTs-TiO_2/EG	T, φ μ_{nf}	25–55 °C up to 1 vol.%	$R^2 = 0.995$	RSM
Tian et al. [60]	CuO/MWCNTs into water/EG	T, φ μ_{nf}	20–60 °C Up to 1 vol.%	$R^2 = 0.9987$	RSM

Table 3 reveals that the methods of estimating GO-CuO/water-EG viscosity have not been investigated. In this study, two different techniques are utilized. The first technique employed the response surface methodology based on the design of experiments. In the second technique, artificial intelligence algorithms are implemented to estimate the GO-CuO/water-EG hybrid nanofluid viscosity. Considering the possibility of non-Newtonian behavior of nanofluid, temperature, shear rate, and volume fraction were effective on the target variable and were defined in the implementation of both techniques. Considering two constraints (i.e, the maximum R-square value and the minimum root mean square error), the best neural network and suitable polynomial were selected. Finally, a comparison was made between the two techniques to evaluate their potential in viscosity estimation.

2. Input Data

In this paper, the GO-CuO/water-EG hybrid nanofluid viscosity is predicted. The nanofluid is prepared from GO as well as CuO and water-EG. μ_{nf} was measured at 25–50 °C (with 5 °C interval) and 0.1, 0.2, 0.4, 0.8, and 1.6 vol%. [61] (Figure 1). In the paper conducted by Rostami et al. [61], the details of morphology, XRD and TEM/SEM images, preparation, and stability were explained. By carefully studying the viscosity changes in terms of shear rates, it is found that the behavior of the hybrid nanofluids is strongly dependent on the amount of added nanoparticles. For $\varphi \leq 0.4$ vol.%, GO-CuO/water-EG hybrid nanofluids are treated like a fluid with Newtonian behavior, while with a further increase in φ, the nanofluids exhibit non-Newtonian behavior [61]. Note that, for a fluid with Newtonian behavior, viscosity is influenced by T as well as φ, while for non-Newtonian behavior, shear rate should be added to the effective parameters.

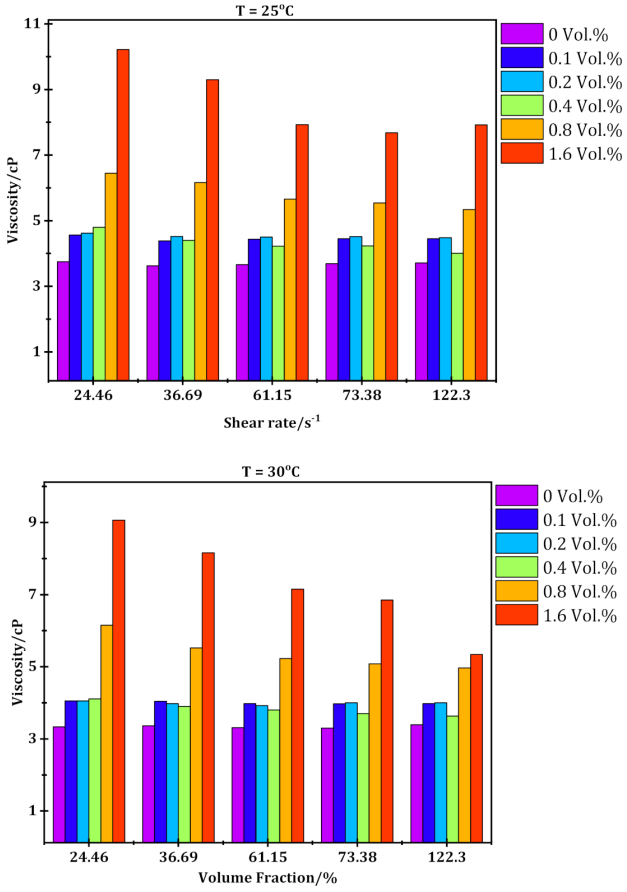

Figure 1. *Cont.*

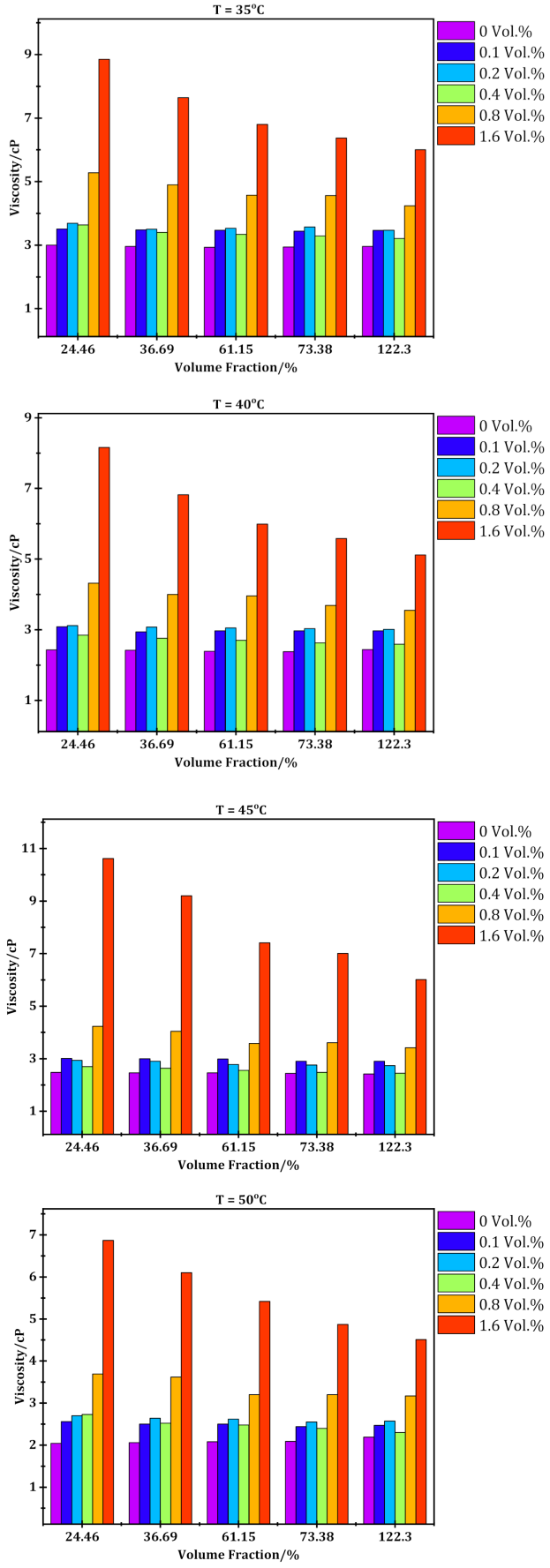

Figure 1. The experimental viscosity.

3. Artificial Neural Network

Artificial neural networks are inspired by the human brain structure and utilized in viscosity prediction by many researchers [62–65]. ANNs consist of three layers: input, hidden, and output layers [66,67]. Each layer contains a group of neurons that are generally associated with all other layer neurons. Note that the neurons of each layer do not interact with other neurons of the same layer. The neuron is the smallest unit performing information processing. It is considered as a basis for ANN. The neuron is considered as a function with nonlinear behavior, so ANNs formed by the assembly of nonlinear functions are completely complex. The number of neurons in the first layer (i.e., input layer) is determined by the number of input variables. Input variables in this study are temperature, viscosity, and shear rate. Hence, the number of input neurons is three (Figure 2). In neural networks, each input (X_i) has a weight that is represented by (W_i). As can be seen, each input is connected to a single weight. Each input must be multiplied by its weight. In the neural network, the result of $(X_i\ W_i)$ is summed by the sigma operator $(\sum X_i W_i)$. The sigma operator output enters the activation function.

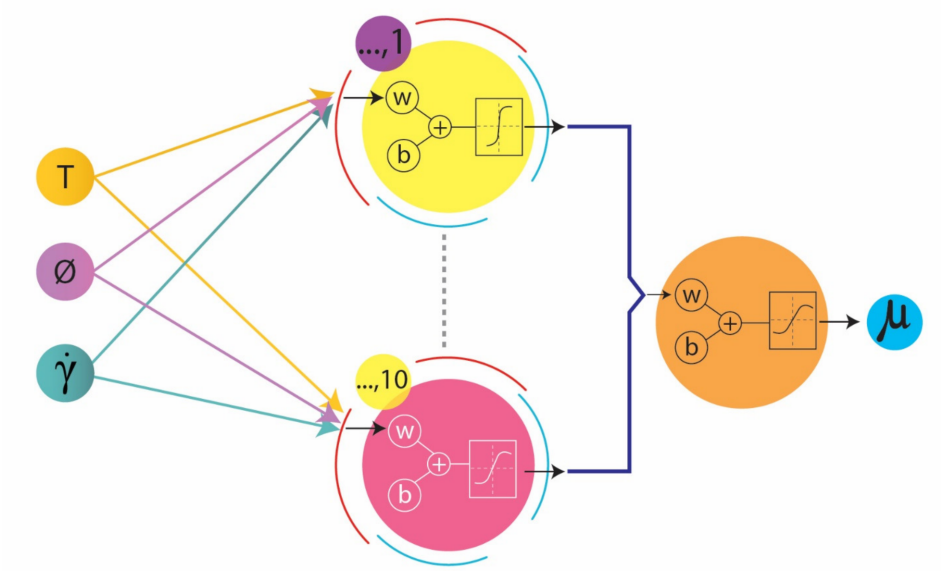

Figure 2. ANN structure.

These functions are a part of neural networks whose input is a number (small or large in arbitrary range), and their output is usually a number between 0 and 1, or −1 and +1. In fact, these functions convert an input number to a specified interval (e.g., −1 to +1). Transfer functions are also called activation functions. The non-linear sigmoid activation function is used in this simulation. In general, the neural network can be considered as a transformation function from a space with n dimension (in the input) to a space with m dimension (in the output). In this study, the neural network converts a three-dimensional input space into a one-dimensional space output. Input space consists of temperature, mass fraction, and shear rate (3D), and output space is only viscosity (1D).

4. RSM

Mathematical methods have many applications in many fields [68–72]. One of the methods for predicting the objective function (e.g., viscosity and thermal conductivity) is the use of response surface methodology [73–77]. In this technique, a polynomial is derived using mathematical and statistical methods to estimate the objective function. In these polynomials, there are either independent variables with the power of 1, 2, and 3 (e.g., T^2) or the combination of multiple independent variables (e.g., T$\dot{\gamma}$). The significance of each independent parameter can be estimated by applying ANOVA. Then, by applying

the concept of regression and considering the values of R-square, the best polynomial correlation is proposed.

5. Results and Discussion

Temperature (T), shear rate $(\dot{\gamma})$, and mass fraction (φ) are identified as input variables and viscosity is the output (objective or target) variable. Using the RSM technique, the following polynomials are suggested for visibility estimation.

$$\begin{aligned}\mu_{nf} = a_0 + a_1\, T \quad & + a_2\, \varphi + a_3\dot{\gamma} + a_4 T\varphi + a_5 T\dot{\gamma} + a_6\varphi\dot{\gamma} + a_7\, T^2 + a_8\, \varphi^2 + a_9\dot{\gamma}^2 \\ & + a_{10} T\varphi\dot{\gamma} + a_{11} T^2\varphi + a_{12} T\dot{\gamma}^2 + a_{13} T\varphi^2 + a_{14} T\dot{\gamma}^2 \\ & + a_{15}\varphi^2\dot{\gamma} + a_{16}\dot{\gamma}^2\varphi + a_{17} T^3 + a_{18}\varphi^3 + a_{19}\dot{\gamma}^3\end{aligned} \tag{1}$$

Table 4 reports the results of ANOVA. If the *p*-value for any parameter is less than 0.05, then it can be said that any variations in that parameter have a substantial result on the target variable, while values higher than 0.1 show that the variation in the parameters has no considerable effect [78]. According to Table 4, the significant parameters are shown in bold.

Table 4. ANOVA results.

p-Value	F-Value	Parameter	*p*-Value	F-Value	Parameter
0.98	0.00058	$T\dot{\gamma}$	< 0.0001	32.95	T
0.153	2.0577	$T\varphi$	< 0.0001	55.026	φ
< 0.0001	123.39	$\dot{\gamma}\varphi$	0.2777	1.1862	$\dot{\gamma}$
0.711	0.1374	$T\dot{\gamma}\varphi$	0.0075	7.313	T^2
0.618	0.25	$T^2\dot{\gamma}$	< 0.0001	22.77	$\dot{\gamma}^2$
0.863	0.0296	$T^2\varphi$	< 0.0001	46.368	φ^2
0.741	0.109	$T\dot{\gamma}^2$	0.055	3.737	T^3
0.0166	5.855	$T\varphi^2$	0.395	0.726	$\dot{\gamma}^3$
< 0.0001	20.611	$\dot{\gamma}^2\varphi$	0.778	0.0794	φ^3
0.0224	5.312	$\dot{\gamma}\varphi^2$			

Table 5 presents the values of $a_0 - a_{19}$. Two criteria of mean square error (MSE) [79,80] and R-square [74,81] can be utilized to assess the proposed correlation performance (Equation (1)):

$$MSE = \frac{1}{N}\sum_{i=1}^{N}\left(\mu_{Pred} - \mu_{Exp}\right)^2 \tag{2}$$

$$-\,square = \left(\frac{\sum_{i=1}^{N}\left(\mu_{Exp} - \overline{\mu}_{exp}\right)\left(\mu_{Pred} - \overline{\mu}_{Pred}\right)}{\sqrt[2]{\sum_{i=1}^{N}\left(\mu_{Exp} - \overline{\mu}_{exp}\right)^2}\sqrt[2]{\sum_{i=1}^{N}\left(\mu_{Pred} - \overline{\mu}_{Pred}\right)^2}}\right)^2 \tag{3}$$

$$correlation coefficient(R) = \left(\frac{\sum_{i=1}^{N}\left(\mu_{Exp} - \overline{\mu}_{exp}\right)\left(\mu_{Pred} - \overline{\mu}_{Pred}\right)}{\sqrt[2]{\sum_{i=1}^{N}\left(\mu_{Exp} - \overline{\mu}_{exp}\right)^2}\sqrt[2]{\sum_{i=1}^{N}\left(\mu_{Pred} - \overline{\mu}_{Pred}\right)^2}}\right) \tag{4}$$

Table 5. Coefficients' value of the proposed correlation.

Parameter	Value	Parameter	Value
a_0	14.914	$\mathbf{a}_{10}$	−7.438 E−5
a_1	−0.78439	$\mathbf{a}_{11}$	−1.620 E−4
a_2	4.26804	$\mathbf{a}_{12}$	7.576 E−6
a_3	−0.0209	$\mathbf{a}_{13}$	0.0383
a_4	−0.054	$\mathbf{a}_{14}$	−1.2028 E−6
a_5	−3.288 E−4	$\mathbf{a}_{15}$	−9.1588 E−3
a_6	−0.039446	$\mathbf{a}_{16}$	2.57 E−4
a_7	0.018264	$\mathbf{a}_{17}$	−1.517 E−4
a_8	0.55451	$\mathbf{a}_{18}$	−0.13075
a_9	4.33736 E−4	$\mathbf{a}_{19}$	−1.908 E−6

Applying Equations (2) and (3), the values of MSE and R-square are 0.166 and 0.944, respectively. The R-square value of 0.944 affirms that the accuracy of the proposed correlation (Equation (1)) is very high and, therefore, the viscosity can be predicted with high accuracy. Another criterion of the suitability of the proposed correlation (Equation (1)) can be obtained by calculating the margin of deviation (*MOD*) [58,79].

$$MOD = \frac{\mu_{Exp} - \mu_{Pred}}{\mu_{Exp}} \times 100 \quad (5)$$

By focusing on Figure 3, it is found that the *MOD* varies in the range of 0 to 24.48%. Thereby, the maximum margin of deviation is 24.48%.

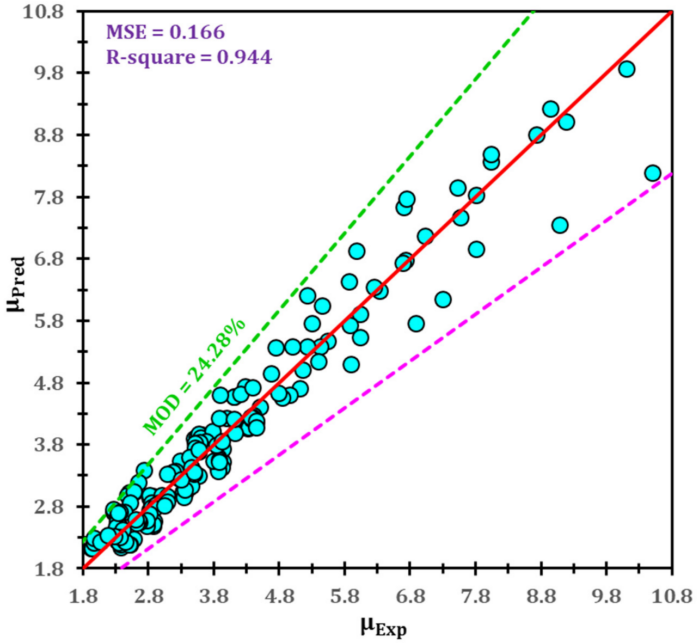

Figure 3. Margin of deviation of proposed correlation (Equation (1)).

However, many researchers also require the maximum amount of residual. The maximum value of the residual can be seen in Figure 4.

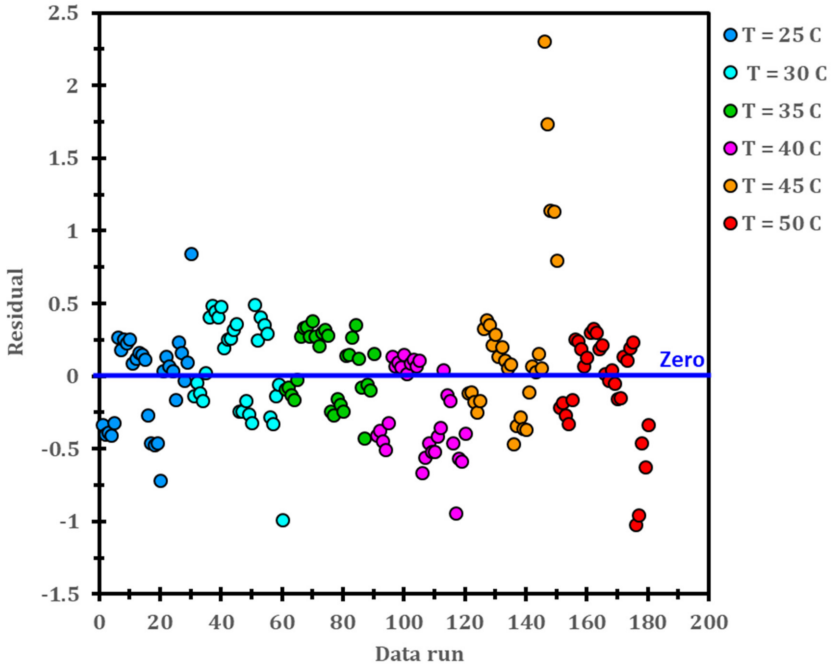

Figure 4. Residual value for the proposed correlation.

The most important criterion for evaluating the accuracy of a correlation is illustrating the predicted value against the laboratory value. In Figure 5, all experimental viscosity (at 180 points) are compared with the predicted viscosity value. At low temperatures, accuracy seems to be poor. Therefore, a comparison was made for each temperature separately. Figure 6 shows the compared μ_{Exp} and μ_{Pred} at each temperature.

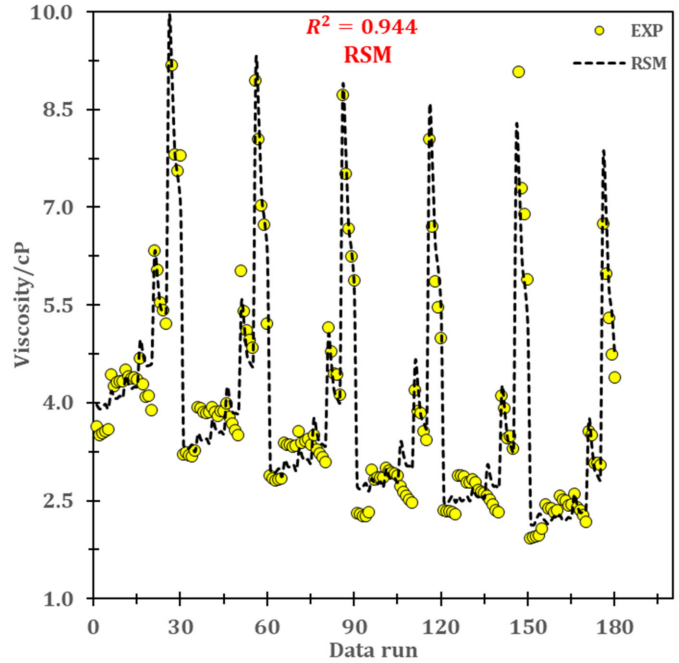

Figure 5. Comparison between μ_{Exp} and μ_{RSM}.

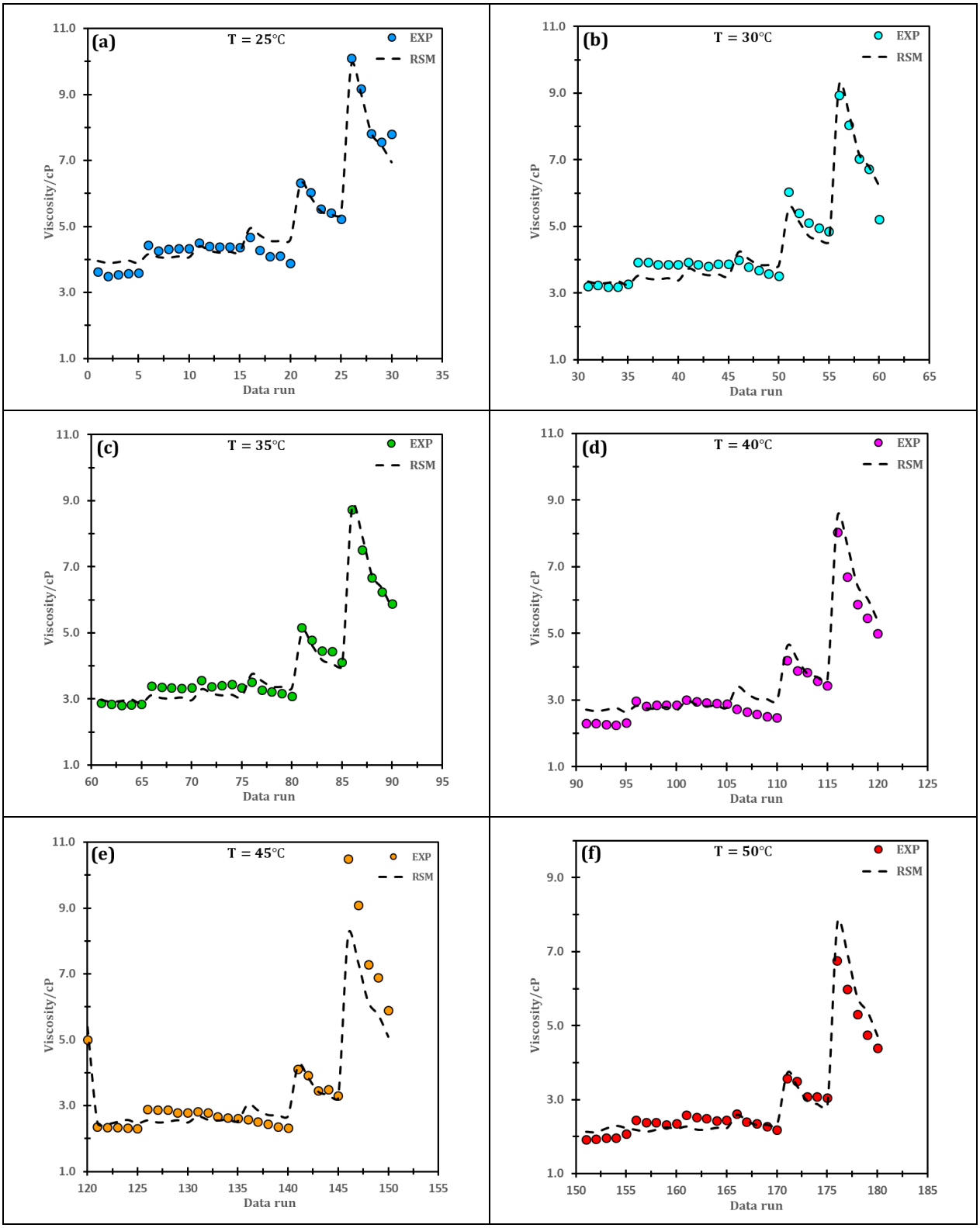

Figure 6. Correlation versus experimental data at different temperatures (RSM method).

As can be seen, for each temperature, some points are not fitted by the correlation. In the following, the results obtained from the ANN method are presented. As mentioned, the ANN method consists of three layers, and Figure 7 shows the amount of correlation coefficient value in all three layers.

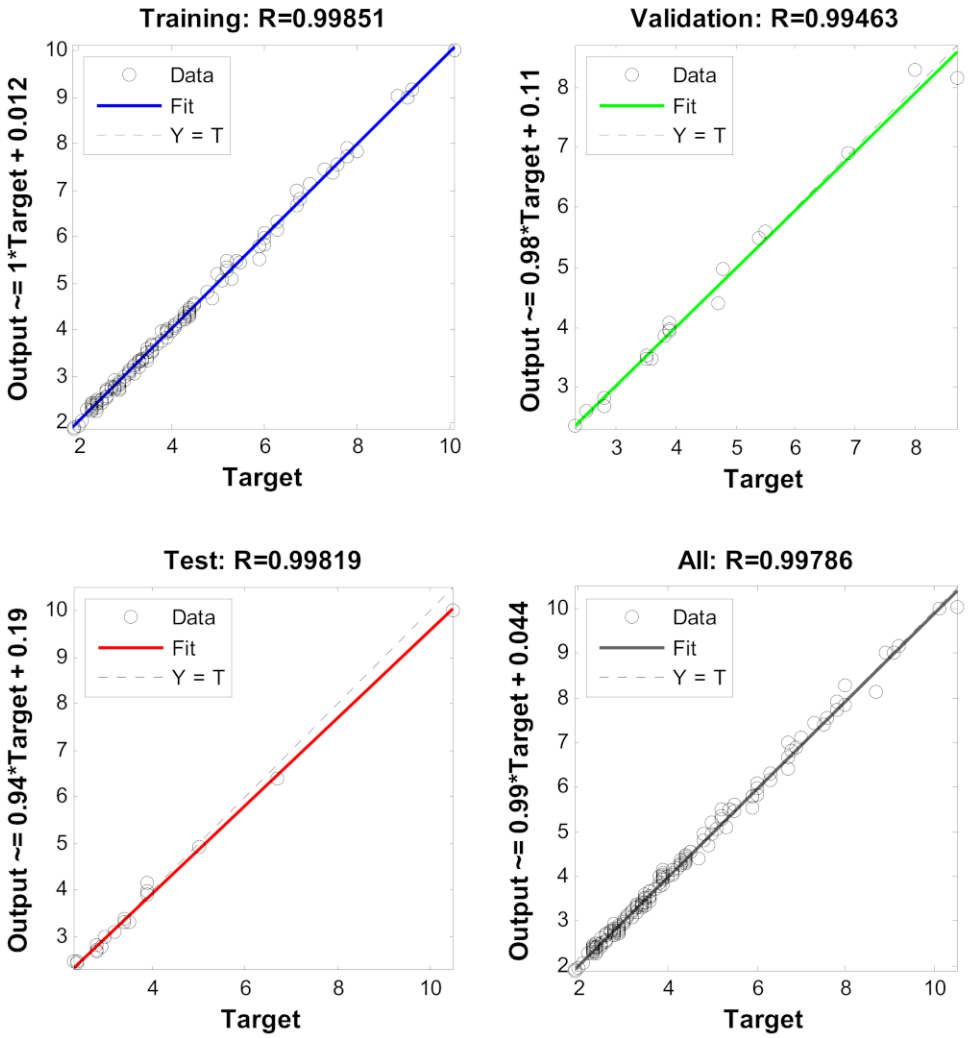

Figure 7. Investigation of accuracy in training, validation, and test sections of neural network algorithm and correlation coefficient values (R).

Note that the R-square for ANN, according to Figure 7, is $0.99786^2 \sim 0.995$. The accuracy of the neural network can be obtained by drawing the output data. In Figure 8, the viscosity value (output from the neural network) is compared with its experimental value.

It is found that the developed ANN can well estimate the viscosity. However, the values of the MOD are reported in Figure 9. As shown, the $MOD_{maximum}$ for the developed neural network is approximately 6.7%. Figure 10 compares the results of ANN and RSM. At all temperatures, ANN accuracy outweighs the accuracy of the RSM method because it fits more points.

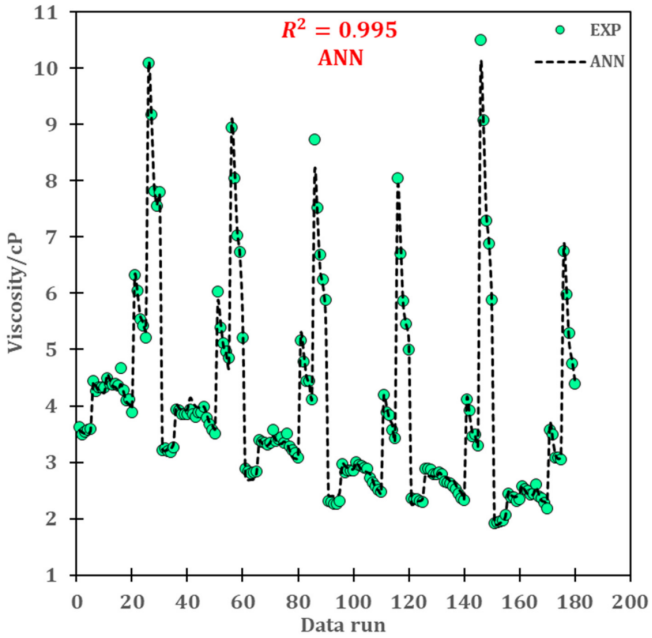

Figure 8. Investigating the ANN accuracy.

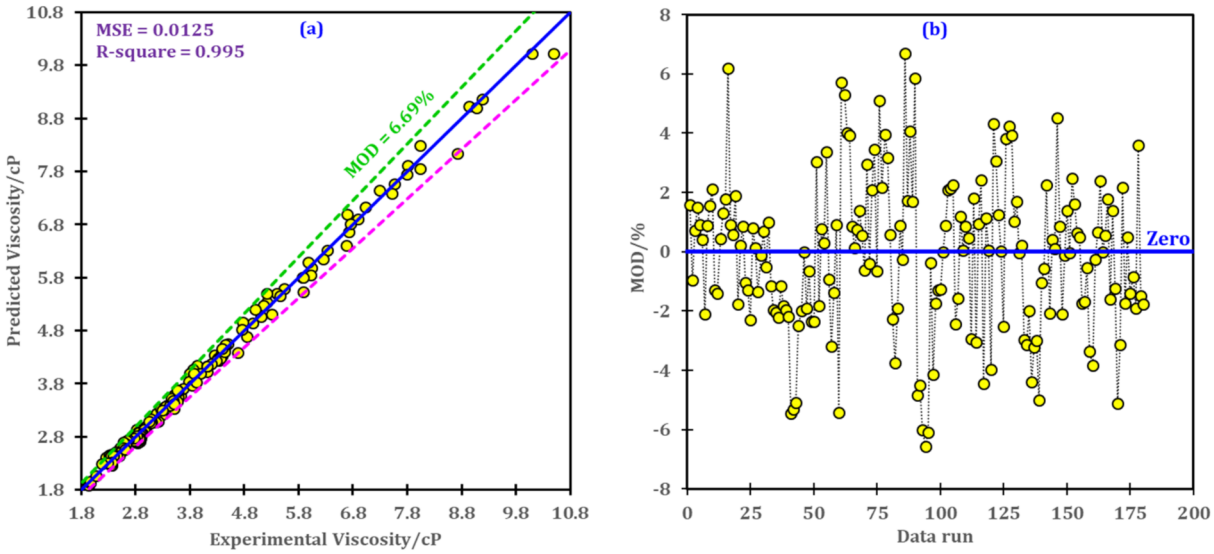

Figure 9. Margin of deviation for the ANN technique.

It should be noted that, for data run within the range of 146–150 in Figure 7e, the fluid has a non-newtonian behavior. Fluid behavior at volume fractions of 0.1, 0.2, and 0.4 is Newtonian and, for 0.8 and 1.6 vol.%, the behavior changed to non-Newtonian [61]. In other words, up to a volume fraction of 0.4, viscosity is not sensitive to one of the input parameters (shear rate), but it is quite sensitive to the shear rate at 0.8 and 1.6 vol.%. Therefore, it is logical that the accuracy of RSM is not high in this range. Therefore, using ANN for nanofluids with changing behavior from Newtonian to non-Newtonian is much better than the RSM method.

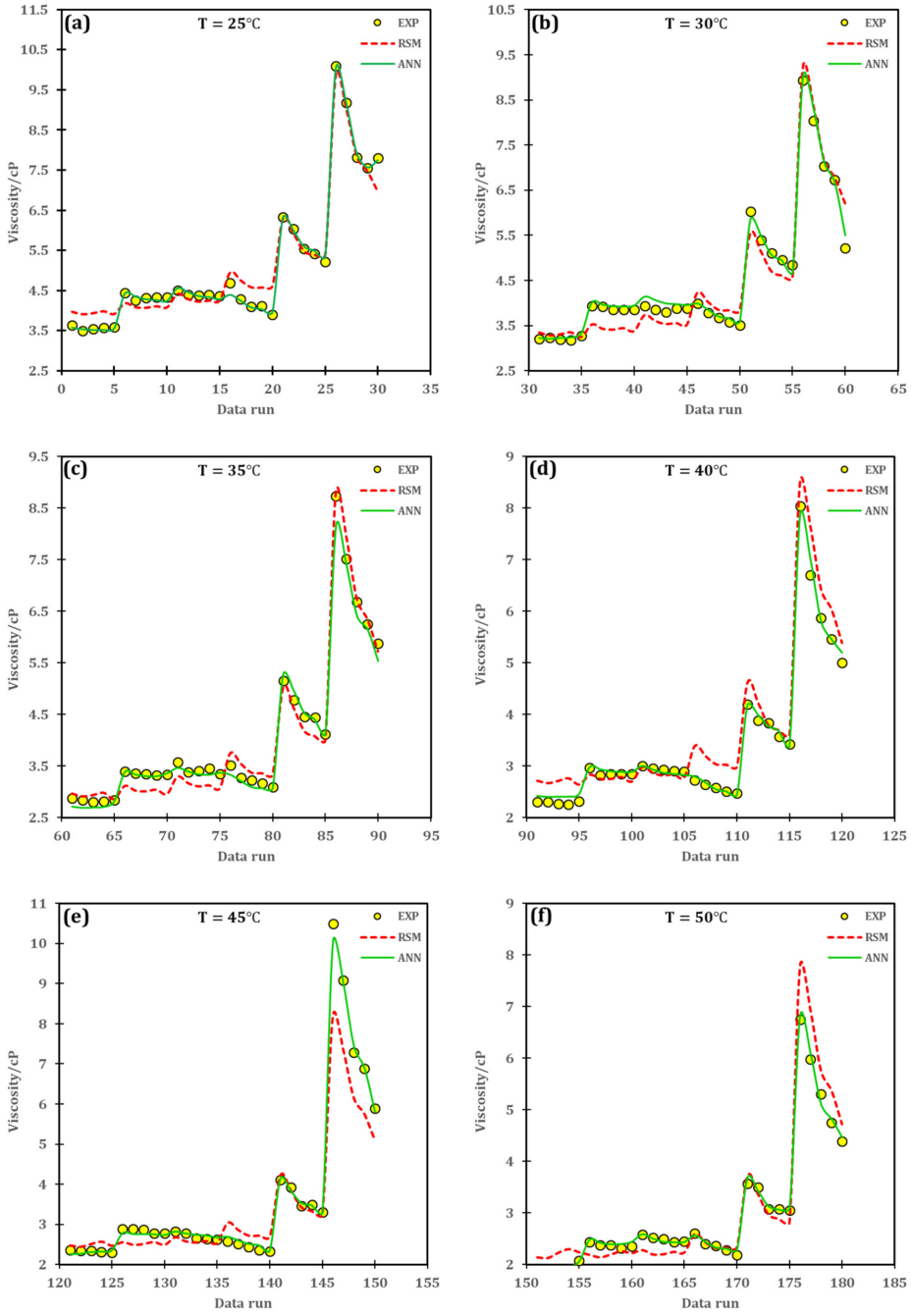

Figure 10. Comparison between ANN and RSM techniques.

6. Conclusions

In this study, the efficacy of loading GO and CuO nanoparticles into EG-water on viscosity was evaluated by applying two numerical techniques. The first technique employed the response surface methodology based on the design of experiments, while in the second technique, artificial intelligence algorithms are implemented to estimate the GO-CuO/water-EG hybrid nanofluid viscosity. Considering the possibility of non-Newtonian behavior of nanofluid, temperature, shear rate, and volume fraction were effective on the target variable and were defined in the implementation of both techniques. Considering two constraints maximizing the R-square as well as minimizing the mean square error, the best neural network and suitable polynomial were approved. It was found that the R-squared for ANN and RSM techniques can reach 0.995 and 0.944, respectively,

and, simultaneously, the mean square error for the approved ANN and RSM techniques was 0.0125 and 0.166, respectively, which indicate that using ANN is prioritized over the RSM technique.

Author Contributions: Data curation, A.A.M. and Y.K.; Formal analysis, Y.K.; Investi-gation, A.A.M. and A.K.A.; Methodology, Y.K. and A.K.A. and S.M.S.; Supervision, M.S. and G.C.; Writing—original draft, Y.K., A.A.M. and A.K.A.; Writing—review & editing, A.A.M., M.S. and G.C.; Conceptu-alization, M.S. and G.C. All authors have read and agreed to the published version of the manuscript.

Funding: This research received no external funding.

Institutional Review Board Statement: Not applicable.

Informed Consent Statement: Not applicable.

Data Availability Statement: Not applicable.

Acknowledgments: This work was supported by the Taif University Researchers Supporting grant number (TURSP-2020/266) of Taif University, Taif, Saudi Arabia.

Conflicts of Interest: The authors declare no conflict of interest.

Nomenclature

ANOVA	Analysisofvariance
ANN	Artificialneuralnetwork
EG	Ethyleneglycol
GO	Grapheneoxide
GON	*Grapheneoxide nanosheets*
GN	*Grapheme nanosheets*
k_{nf}	Nanofluidthermalconductivity/$Wm^{-1}K^{-1}$
k_{bf}	Basefluidthermalconductivity/$Wm^{-1}K^{-1}$
MSE	Meansquareerror
MOD	Marginofdeviation
MWCNTs	$Multi-walledcarbonnanotubes$
RSM	Responsesurfacemethodology
T	Temperature/°C
TCR	Thermalconductivityratio
Greek letter	
φ	Volumefraction/%
$\dot{\gamma}$	Shearrate/s^{-1}
μ	Viscosity/cP

References

1. Khan, M.S.; Amber, K.P.; Ali, H.M.; Abid, M.; Ratlamwala, T.A.; Javed, S. Performance analysis of solar assisted multigenerational system using therminol VP1 based nanofluids: A comparative study. *Therm. Sci.* **2020**, *24*, 865–878. [CrossRef]
2. Salimpour, M.R.; Kalbasi, R.; Lorenzini, G. Constructal multi-scale structure of PCM-based heat sinks. *Contin. Mech. Thermodyn.* **2017**, *29*, 477–491. [CrossRef]
3. Khan, M.S.; Abid, M.; Ali, H.M.; Amber, K.P.; Bashir, M.A.; Javed, S. Comparative performance assessment of solar dish assisted s-CO_2 Brayton cycle using nanofluids. *Appl. Therm. Eng.* **2019**, *148*, 295–306. [CrossRef]
4. Khan, M.S.; Yan, M.; Ali, H.M.; Amber, K.P.; Bashir, M.A.; Akbar, B.; Javed, S. Comparative performance assessment of different absorber tube geometries for parabolic trough solar collector using nanofluid. *J. Therm. Anal. Calorim.* **2020**, *142*, 2227–2241. [CrossRef]
5. Ali, H.M.; Babar, H.; Shah, T.R.; Sajid, M.U.; Qasim, M.A.; Javed, S. Preparation Techniques of TiO_2 Nanofluids and Challenges: A Review. *Appl. Sci.* **2018**, *8*, 587. [CrossRef]
6. Motamedi, M.; Naghdi, A.; Jalali, S. Effect of temperature on properties of aluminum/single-walled carbon nanotube nanocomposite by molecular dynamics simulation. *J. Mech. Eng. Sci.* **2019**, *234*, 635–642. [CrossRef]
7. Giwa, S.O.; Sharifpur, M.; Ahmadi, M.H.; Meyer, J. Magnetohydrodynamic convection behaviours of nanofluids in non-square enclosures: A comprehensive review. *Math. Methods Appl. Sci.* **2020**. [CrossRef]
8. Giwa, S.O.; Sharifpur, M.; Ahmadi, M.H.; Meyer, J.P. A review of magnetic field influence on natural convection heat transfer performance of nanofluids in square cavities. *J. Therm. Anal. Calorim.* **2021**, *145*, 2581–2623. [CrossRef]

9. Li, Z.; Sarafraz, M.; Mazinani, A.; Hayat, T.; Alsulami, H.; Goodarzi, M. Pool boiling heat transfer to CuO-H_2O nanofluid on finned surfaces. *Int. J. Heat Mass Transf.* **2020**, *156*, 119780. [CrossRef]
10. Mahdavi, M.; Garbadeen, I.; Sharifpur, M.; Ahmadi, M.H.; Meyer, J.P. Study of particle migration and deposition in mixed convective pipe flow of nanofluids at different inclination angles. *J. Therm. Anal. Calorim.* **2019**, *135*, 1563–1575. [CrossRef]
11. Mahdavi, M.; Sharifpur, M.; Ahmadi, M.H.; Meyer, J.P. Aggregation study of Brownian nanoparticles in convective phenomena. *J. Therm. Anal. Calorim.* **2019**, *135*, 111–121. [CrossRef]
12. Nwosu, P.N.; Meyer, J.; Sharifpur, M. Nanofluid Viscosity: A simple model selection algorithm and parametric evaluation. *Comput. Fluids* **2014**, *101*, 241–249. [CrossRef]
13. Arıkan, E.; Abbasoğlu, S.; Gazi, M. Experimental Performance Analysis of Flat Plate Solar Collectors Using Different Nanofluids. *Sustainability* **2018**, *10*, 1794. [CrossRef]
14. Javed, S.; Ali, H.M.; Babar, H.; Khan, M.S.; Janjua, M.M.; Bashir, M.A. Internal convective heat transfer of nanofluids in different flow regimes: A comprehensive review. *Phys. A Stat. Mech. Its Appl.* **2020**, *538*, 122783. [CrossRef]
15. Ahmadi, M.H.; Mohseni-Gharyehsafa, B.; Ghazvini, M.; Goodarzi, M.; Jilte, R.; Kumar, R. Comparing various machine learning approaches in modeling the dynamic viscosity of CuO/water nanofluid. *J. Therm. Anal. Calorim.* **2019**, *139*, 2585–2599. [CrossRef]
16. Kalbasi, R. Introducing a novel heat sink comprising PCM and air—Adapted to electronic device thermal management. *Int. J. Heat Mass Transf.* **2021**, *169*, 120914. [CrossRef]
17. Bahiraei, M.; Heshmatian, S. Graphene family nanofluids: A critical review and future research directions. *Energy Convers. Manag.* **2019**, *196*, 1222–1256. [CrossRef]
18. Arshad, A.; Jabbal, M.; Yan, Y.; Reay, D. A review on graphene based nanofluids: Preparation, characterization and applications. *J. Mol. Liq.* **2019**, *279*, 444–484. [CrossRef]
19. Motamedi, M.; Naghdi, A.; Sohail, A.; Li, Z. Effect of elastic foundation on vibrational behavior of graphene based on first-order shear deformation theory. *Adv. Mech. Eng.* **2018**, *10*, 1687814018814624. [CrossRef]
20. Sadeghinezhad, E.; Mehrali, M.; Saidur, R.; Mehrali, M.; Latibari, S.T.; Akhiani, A.R.; Metselaar, H.S.C. A comprehensive review on graphene nanofluids: Recent research, development and applications. *Energy Convers. Manag.* **2016**, *111*, 466–487. [CrossRef]
21. Hu, Y.; Li, H.; He, Y.; Wang, L. Role of nanoparticles on boiling heat transfer performance of ethylene glycol aqueous solution based graphene nanosheets nanofluid. *Int. J. Heat Mass Transf.* **2016**, *96*, 565–572. [CrossRef]
22. Yu, W.; Xie, H.; Chen, L.; Li, Y.; Li, D. The Preparation and Thermal Conductivities Enhacement of Nanofluids Containing Graphene Oxide Nanosheets. In Proceedings of the 2010 14th International Heat Transfer Conference, Washington, DC, USA, 8–13 August 2010; pp. 569–573.
23. Yu, W.; Xie, H.; Chen, W. Experimental investigation on thermal conductivity of nanofluids containing graphene oxide nanosheets. *J. Appl. Phys.* **2010**, *107*, 094317. [CrossRef]
24. Yu, W.; Xie, H.; Bao, D. Enhanced thermal conductivities of nanofluids containing graphene oxide nanosheets. *Nanotechnology* **2009**, *21*, 055705. [CrossRef]
25. Yu, W.; Xie, H.; Wang, X.; Wang, X. Significant thermal conductivity enhancement for nanofluids containing graphene nanosheets. *Phys. Lett. A* **2011**, *375*, 1323–1328. [CrossRef]
26. Moghaddam, M.B.; Goharshadi, E.; Entezari, M.H.; Nancarrow, P. Preparation, characterization, and rheological properties of graphene–glycerol nanofluids. *Chem. Eng. J.* **2013**, *231*, 365–372. [CrossRef]
27. Ahammed, N.; Asirvatham, G.; Titus, J.; Bose, J.R.; Wongwises, S. Measurement of thermal conductivity of graphene–water nanofluid at below and above ambient temperatures. *Int. Commun. Heat Mass Transf.* **2016**, *70*, 66–74. [CrossRef]
28. Baby, T.T.; Ramaprabhu, S. Enhanced convective heat transfer using graphene dispersed nanofluids. *Nanoscale Res. Lett.* **2011**, *6*, 289. [CrossRef]
29. Aravind, S.S.J.; Ramaprabhu, S. Surfactant free graphene nanosheets based nanofluids by in-situ reduction of alkaline graphite oxide suspensions. *J. Appl. Phys.* **2011**, *110*, 124326. [CrossRef]
30. Kole, M.; Dey, T.K. Investigation of thermal conductivity, viscosity, and electrical conductivity of graphene based nanofluids. *J. Appl. Phys.* **2013**, *113*, 084307. [CrossRef]
31. Águila, B.; Vasco, D.A.; Galvez, P.; Zapata, P.A. Effect of temperature and CuO-nanoparticle concentration on the thermal conductivity and viscosity of an organic phase-change material. *Int. J. Heat Mass Transf.* **2018**, *120*, 1009–1019. [CrossRef]
32. Sahoo, R.R.; Kumar, V. Development of a new correlation to determine the viscosity of ternary hybrid nanofluid. *Int. Commun. Heat Mass Transf.* **2020**, *111*, 104451. [CrossRef]
33. Esfe, M.H.; Zabihi, F.; Rostamian, H.; Esfandeh, S. Experimental investigation and model development of the non-Newtonian behavior of CuO-MWCNT-10w40 hybrid nano-lubricant for lubrication purposes. *J. Mol. Liq.* **2018**, *249*, 677–687. [CrossRef]
34. Akilu, S.; Baheta, A.T.; Sharma, K. Experimental measurements of thermal conductivity and viscosity of ethylene glycol-based hybrid nanofluid with TiO_2-CuO/C inclusions. *J. Mol. Liq.* **2017**, *246*, 396–405. [CrossRef]
35. Asadi, A.; Alarifi, I.M.; Foong, L.K. An experimental study on characterization, stability and dynamic viscosity of CuO-TiO_2/water hybrid nanofluid. *J. Mol. Liq.* **2020**, *307*, 112987. [CrossRef]
36. Shah, J.; Kumar, S.; Ranjan, M.; Sonvane, Y.; Thareja, P.; Gupta, S.K. The effect of filler geometry on thermo-optical and rheological properties of CuO nanofluid. *J. Mol. Liq.* **2018**, *272*, 668–675. [CrossRef]
37. Priya, K.R.; Suganthi, K.; Rajan, K. Transport properties of ultra-low concentration CuO–water nanofluids containing non-spherical nanoparticles. *Int. J. Heat Mass Transf.* **2012**, *55*, 4734–4743. [CrossRef]

38. Alawi, O.A.; Sidik, N.A.C. Influence of particle concentration and temperature on the thermophysical properties of CuO/R134a nanorefrigerant. *Int. Commun. Heat Mass Transf.* **2014**, *58*, 79–84. [CrossRef]
39. Çolak, A.B.; Yıldız, O.; Bayrak, M.; Celen, A.; Dalkılıç, A.S.; Wongwises, S. Experimental Study on the Specific Heat Capacity Measurement of Water- Based Al2O3-Cu Hybrid Nanofluid by using Differential Thermal Analysis Method. *Curr. Nanosci.* **2021**, *16*, 912–928. [CrossRef]
40. Yan, S.-R.; Kalbasi, R.; Nguyen, Q.; Karimipour, A. Rheological behavior of hybrid MWCNTs-TiO2/EG nanofluid: A comprehensive modeling and experimental study. *J. Mol. Liq.* **2020**, *308*, 113058. [CrossRef]
41. Çolak, A.B.; Yıldız, O.; Bayrak, M.; Tezekici, B.S. Experimental study for predicting the specific heat of water based Cu-Al_2O_3 hybrid nanofluid using artificial neural network and proposing new correlation. *Int. J. Energy Res.* **2020**, *44*, 7198–7215. [CrossRef]
42. Giwa, S.O.; Sharifpur, M.; Goodarzi, M.; Alsulami, H.; Meyer, J.P. Influence of base fluid, temperature, and concentration on the thermophysical properties of hybrid nanofluids of alumina–ferrofluid: Experimental data, modeling through enhanced ANN, ANFIS, and curve fitting. *J. Therm. Anal. Calorim.* **2021**, *143*, 4149–4167. [CrossRef]
43. Khosravi, R.; Rabiei, S.; Khaki, M.; Safaei, M.R.; Goodarzi, M. Entropy generation of graphene-platinum hybrid nanofluid flow through a wavy cylindrical microchannel solar receiver by using neural networks. *J. Therm. Anal. Calorim.* **2021**, *145*, 1949–1967. [CrossRef]
44. Peng, Y.; Parsian, A.; Khodadadi, H.; Akbari, M.; Ghani, K.; Goodarzi, M.; Bach, Q.-V. Develop optimal network topology of artificial neural network (AONN) to predict the hybrid nanofluids thermal conductivity according to the empirical data of Al2O3—Cu nanoparticles dispersed in ethylene glycol. *Phys. A Stat. Mech. Its Appl.* **2020**, *549*, 124015. [CrossRef]
45. Karimipour, A.; Bagherzadeh, S.A.; Goodarzi, M.; Alnaqi, A.A.; Bahiraei, M.; Safaei, M.R.; Shadloo, M.S. Synthesized $CuFe_2O_4/SiO_2$ nanocomposites added to water/EG: Evaluation of the thermophysical properties beside sensitivity analysis & EANN. *Int. J. Heat Mass Transf.* **2018**, *127*, 1169–1179.
46. Alrashed, A.A.; Gharibdousti, M.S.; Goodarzi, M.; de Oliveira, L.R.; Safaei, M.R.; Filho, E.B. Effects on thermophysical properties of carbon based nanofluids: Experimental data, modelling using regression, ANFIS and ANN. *Int. J. Heat Mass Transf.* **2018**, *125*, 920–932. [CrossRef]
47. Bagherzadeh, S.A.; D'Orazio, A.; Karimipour, A.; Goodarzi, M.; Bach, Q.-V. A novel sensitivity analysis model of EANN for F-MWCNTs–Fe_3O_4/EG nanofluid thermal conductivity: Outputs predicted analytically instead of numerically to more accuracy and less costs. *Phys. A Stat. Mech. Its Appl.* **2019**, *521*, 406–415. [CrossRef]
48. Ghasemi, A.; Hassani, M.; Goodarzi, M.; Afrand, M.; Manafi, S. Appraising influence of COOH-MWCNTs on thermal conductivity of antifreeze using curve fitting and neural network. *Phys. A Stat. Mech. Its Appl.* **2019**, *514*, 36–45. [CrossRef]
49. Esfe, M.H.; Saedodin, S.; Naderi, A.; Alirezaie, A.; Karimipour, A.; Wongwises, S.; Goodarzi, M.; bin Dahari, M. Modeling of thermal conductivity of ZnO-EG using experimental data and ANN methods. *Int. Commun. Heat Mass Transf.* **2015**, *63*, 35–40. [CrossRef]
50. Hosseini, S.M.; Safaei, M.R.; Goodarzi, M.; Alrashed, A.A.; Nguyen, T.K. New temperature, interfacial shell dependent dimensionless model for thermal conductivity of nanofluids. *Int. J. Heat Mass Transf.* **2017**, *114*, 207–210. [CrossRef]
51. Bahrami, M.; Akbari, M.; Bagherzadeh, S.A.; Karimipour, A.; Afrand, M.; Goodarzi, M. Develop 24 dissimilar ANNs by suitable architectures & training algorithms via sensitivity analysis to better statistical presentation: Measure MSEs between targets & ANN for Fe–CuO/Eg–Water nanofluid. *Phys. A Stat. Mech. Its Appl.* **2019**, *519*, 159–168. [CrossRef]
52. Shamshirband, S.; Malvandi, A.; Karimipour, A.; Goodarzi, M.; Afrand, M.; Petković, D.; Dahari, M.; Mahmoodian, N. Performance investigation of micro-and nano-sized particle erosion in a 90 elbow using an ANFIS model. *Powder Technol.* **2015**, *284*, 336–343. [CrossRef]
53. Wu, H.; Bagherzadeh, S.A.; D'Orazio, A.; Habibollahi, N.; Karimipour, A.; Goodarzi, M.; Bach, Q.-V. Present a new multi objective optimization statistical Pareto frontier method composed of artificial neural network and multi objective genetic algorithm to improve the pipe flow hydrodynamic and thermal properties such as pressure drop and heat transfer coefficient for non-Newtonian binary fluids. *Phys. A Stat. Mech. Its Appl.* **2019**, *535*, 122409. [CrossRef]
54. Zhao, N.; Wen, X.; Yang, J.; Li, S.; Wang, Z. Modeling and prediction of viscosity of water-based nanofluids by radial basis function neural networks. *Powder Technol.* **2015**, *281*, 173–183. [CrossRef]
55. Shahsavar, A.; Bahiraei, M. Experimental investigation and modeling of thermal conductivity and viscosity for non-Newtonian hybrid nanofluid containing coated CNT/Fe_3 O_4 nanoparticles. *Powder Technol.* **2017**, *318*, 441–450. [CrossRef]
56. Ghaffarkhah, A.; Bazzi, A.; Dijvejin, Z.A.; Talebkeikhah, M.; Moraveji, M.K.; Agin, F. Experimental and numerical analysis of rheological characterization of hybrid nano-lubricants containing COOH-Functionalized MWCNTs and oxide nanoparticles. *Int. Commun. Heat Mass Transf.* **2019**, *101*, 103–115. [CrossRef]
57. Alirezaie, A.; Saedodin, S.; Esfe, M.H.; Rostamian, S.H. Investigation of rheological behavior of MWCNT (COOH-functionalized)/MgO—Engine oil hybrid nanofluids and modelling the results with artificial neural networks. *J. Mol. Liq.* **2017**, *241*, 173–181. [CrossRef]
58. Yan, S.-R.; Kalbasi, R.; Nguyen, Q.; Karimipour, A. Sensitivity of adhesive and cohesive intermolecular forces to the incorporation of MWCNTs into liquid paraffin: Experimental study and modeling of surface tension. *J. Mol. Liq.* **2020**, *310*, 113235. [CrossRef]
59. Tian, X.-X.; Kalbasi, R.; Qi, C.; Karimipour, A.; Huang, H.-L. Efficacy of hybrid nano-powder presence on the thermal conductivity of the engine oil: An experimental study. *Powder Technol.* **2020**, *369*, 261–269. [CrossRef]

60. Tian, Z.; Rostami, S.; Taherialekouhi, R.; Karimipour, A.; Moradikazerouni, A.; Yarmand, H.; Zulkifli, N.W.B.M. Prediction of rheological behavior of a new hybrid nanofluid consists of copper oxide and multi wall carbon nanotubes suspended in a mixture of water and ethylene glycol using curve-fitting on experimental data. *Phys. A Stat. Mech. Its Appl.* **2020**, *549*, 124101. [CrossRef]
61. Rostami, S.; Nadooshan, A.A.; Raisi, A. The effect of hybrid nano-additive consists of graphene oxide and copper oxide on rheological behavior of a mixture of water and ethylene glycol. *J. Therm. Anal. Calorim.* **2019**, *139*, 2353–2364. [CrossRef]
62. Heidari, E.; Sobati, M.A.; Movahedirad, S. Accurate prediction of nanofluid viscosity using a multilayer perceptron artificial neural network (MLP-ANN). *Chemom. Intell. Lab. Syst.* **2016**, *155*, 73–85. [CrossRef]
63. Toghraie, D.; Sina, N.; Jolfaei, N.A.; Hajian, M.; Afrand, M. Designing an Artificial Neural Network (ANN) to predict the viscosity of Silver/Ethylene glycol nanofluid at different temperatures and volume fraction of nanoparticles. *Phys. A Stat. Mech. Its Appl.* **2019**, *534*, 122142. [CrossRef]
64. Esfe, M.H.; Kamyab, M.H.; Afrand, M.; Amiri, M.K. Using artificial neural network for investigating of concurrent effects of multi-walled carbon nanotubes and alumina nanoparticles on the viscosity of 10W-40 engine oil. *Phys. A Stat. Mech. Its Appl.* **2018**, *510*, 610–624. [CrossRef]
65. Zolghadri, A.; Maddah, H.; Ahmadi, M.; Sharifpur, M. Predicting Parameters of Heat Transfer in a Shell and Tube Heat Exchanger Using Aluminum Oxide Nanofluid with Artificial Neural Network (ANN) and Self-Organizing Map (SOM). *Sustainability* **2021**, *13*, 8824. [CrossRef]
66. Shafiq, A.; Çolak, A.B.; Sindhu, T.N.; Al-Mdallal, Q.M.; Abdeljawad, T. Estimation of unsteady hydromagnetic Williamson fluid flow in a radiative surface through numerical and artificial neural network modeling. *Sci. Rep.* **2021**, *11*, 1–21. [CrossRef] [PubMed]
67. Shafiq, A.; Çolak, A.B.; Sindhu, T.N. Designing artificial neural network of nanoparticle diameter and solid–fluid interfacial layer on single-walled carbon nanotubes/ethylene glycol nanofluid flow on thin slendering needles. *Int. J. Numer. Methods Fluids* **2021**. [CrossRef]
68. Rafiee, M.; Abbasian-Naghneh, S. E-learning: Development of a model to assess the acceptance and readiness of technology among language learners. *Comput. Assist. Lang. Learn.* **2019**, 730–750. [CrossRef]
69. Abbasian-Naghneh, S.; Tehrani, R.; Tamimi, M. The Effect of JCPOA on the Network Behavior Analysis of Tehran Stock Exchange Indexes. *Adv. Math. Financ. Appl.* **2019**, *6*, 1–13. [CrossRef]
70. Abbasian-Naghneh, S. Global Malmquist Productivity Index based on preference common-weights. *Filomat* **2016**, *30*, 2653–2661. [CrossRef]
71. Ghanbari, A.; Hadavandi, E.; Abbasian-Naghneh, S. An Intelligent ACO-SA Approach for Short Term Electricity Load Prediction. In Proceedings of the 6th International Conference on Intelligent Computing, ICIC 2010, Changsha, China, 18–21 August 2010; pp. 623–633.
72. Jahanshahloo, G.; Zohrehbandian, M.; Abbasian, H.; Abbasian-Naghneh, S. A new approach for the facility layout design in manufacturing systems. *Life Sci. J.* **2013**, *10*, 1097–8135.
73. Chu, Y.-M.; Ibrahim, M.; Saeed, T.; Berrouk, A.S.; Algehyne, E.A.; Kalbasi, R. Examining rheological behavior of MWCNT-TiO2/5W40 hybrid nanofluid conducting experimental study- Challenging of RSM and ANN. *J. Mol. Liq.* **2021**, *333*, 115969. [CrossRef]
74. Rostami, S.; Kalbasi, R.; Jahanshahi, R.; Qi, C.; Abbasian-Naghneh, S.; Karimipour, A. Effect of silica nano-materials on the viscosity of ethylene glycol: An experimental study by considering sonication duration effect. *J. Mater. Res. Technol.* **2020**, *9*, 11905–11917. [CrossRef]
75. Ibrahim, M.; Saeed, T.; Chu, Y.-M.; Ali, H.M.; Cheraghian, G.; Kalbasi, R. Comprehensive study concerned graphene nano-sheets dispersed in ethylene glycol: Experimental study and theoretical prediction of thermal conductivity. *Powder Technol.* **2021**, *386*, 51–59. [CrossRef]
76. Cheraghian, G. Improved Heavy Oil Recovery by Nanofluid Surfactant Flooding—An Experimental Study. In Proceedings of the 78th EAGE Conference and Exhibition 2016, Online, 30 May–2 June 2016. [CrossRef]
77. Cheraghian, G.; Nezhad, S.S.K.; Bazgir, S. Improvement of thermal stability of polyacryl amide solution used as a nano-fluid in enhanced oil recovery process by nanoclay. *Int. J. Nanosci. Nanotechnol.* **2015**, *11*, 201–208.
78. Kalbasi, R.; Afrand, M.; Alsarraf, J.; Tran, M.-D. Studies on optimum fins number in PCM-based heat sinks. *Energy* **2019**, *171*, 1088–1099. [CrossRef]
79. Tian, X.-X.; Kalbasi, R.; Jahanshahi, R.; Qi, C.; Huang, H.-L.; Rostami, S. Competition between intermolecular forces of adhesion and cohesion in the presence of graphene nanoparticles: Investigation of graphene nanosheets/ethylene glycol surface tension. *J. Mol. Liq.* **2020**, *311*, 113329. [CrossRef]
80. Khetib, Y.; Sedraoui, K.; Gari, A. Improving thermal conductivity of a ferrofluid-based nanofluid using Fe_3O_4- challenging of RSM and ANN methodologies. *Chem. Eng. Commun.* **2021**, *10*, 1–12. [CrossRef]
81. Rostami, S.; Kalbasi, R.; Talebkeikhah, M.; Goldanlou, A.S. Improving the thermal conductivity of ethylene glycol by addition of hybrid nano-materials containing multi-walled carbon nanotubes and titanium dioxide: Applicable for cooling and heating. *J. Therm. Anal. Calorim.* **2021**, *143*, 1701–1712. [CrossRef]